1-1-2007

Amorphous carbon-coated silicon nanocomposites: a low-temperature synthesis via spray pyrolysis and their application as high-capacity anodes for lithium-ion batteries

See How Ng
University of Wollongong, shn076@uow.edu.au

Jiazhao Wang
University of Wollongong, jiazhao@uow.edu.au

David Wexler
University of Wollongong, david_wexler@uow.edu.au

Sau Yen Chew
University of Wollongong, syc410@uow.edu.au

Hua-Kun Liu
University of Wollongong, hua@uow.edu.au

Amorphous Carbon-Coated Silicon Nanocomposites: A Low-Temperature Synthesis via Spray Pyrolysis and Their Application as High-Capacity Anodes for Lithium-Ion Batteries

See How Ng,*,†,‡,# Jiazhao Wang,†,‡ David Wexler,§ Sau Yen Chew,†,‡ and Hua Kun Liu†,‡

Institute for Superconducting and Electronic Materials, ARC Center of Excellence for Electromaterials Science, and Faculty of Engineering, University of Wollongong, NSW 2522, Australia

Received: April 10, 2007; In Final Form: May 20, 2007

This article introduces an effective, inexpensive, and industrially oriented approach to produce carbon-coated Si nanocomposites as high-capacity anode materials for use in rechargeable lithium-ion batteries. Initially, nanosized Si particles (<100 nm) were mixed in a citric acid/ethanol solution via ultrasonication. This mixture was further spray-pyrolyzed in air at low processing temperature (300−500 °C), resulting in a homogeneous layer of carbon coating on the surface of the spheroidal Si nanoparticles. The effects of the processing temperature on the amorphous carbon content, the thickness of the carbon-coating layer, and the homogeneity of the carbon coating were studied in detail. These parameters strongly influenced the electrochemical performance of the carbon-coated Si nanocomposites, as will be discussed below. Carbon-coated Si nanocomposites spray-pyrolyzed in air at 400 °C show the best cycling performance, retaining a specific capacity of 1120 mA·h g^{-1} beyond 100 cycles, with a capacity fading of less than 0.4% per cycle. The beneficial effect of the carbon coating in enhancing the dimensional stability of the Si nanoparticles appears to be the main reason for this markedly improved electrochemical performance.

1. Introduction

Lithium-ion batteries are now the most widely used secondary battery systems for portable electronic devices. In comparison to conventional aqueous rechargeable batteries, such as nickel−cadmium and nickel metal hydride, lithium-ion batteries have higher energy density, higher operating voltages, lower self-discharge, and lower maintenance requirements.[1] These properties have made Li-ion batteries the highest performing secondary battery chemistry available. However, due to the rapid advances and highly competitive nature of the portable devices industry, a further increase in the mass capacities (W·h kg^{-1}) and energy densities (W·h L^{-1}) of the Li-ion rechargeable batteries is being vigorously pursued.

Graphite materials are currently used as anode materials for rechargeable lithium-ion batteries, in which lithium ions intercalate in and out reversibly. Graphite materials provide high electronic conductivity and low electrochemical potential with respect to lithium metal. Yet these superb properties can hardly meet the demand for high energy density from current electronic devices; research on alternative anodes is therefore focused on materials with higher lithium storage capacities. Among the candidates, metals that alloy with lithium are promising alternative anode materials due to their high specific capacities, e.g., Si (4200 mA·h g^{-1})[2] and Sn (994 mA·h g^{-1}),[3] as compared to graphite, which gives a theoretical capacity of 372 mA·h g^{-1}.[4]

However, a general disadvantage is the large volume expansion/contraction[5] during the alloying/dealloying of lithium, resulting in the formation of cracks followed by pulverization of the active mass particles and permanent capacity loss. Studies of the Li−Si binary system[6,7] have indicated that each silicon atom can accommodate up to 4.4 lithium atoms leading to the formation of $Li_{22}Si_5$ alloy, accompanied by a volume expansion of 400%. This huge volume change would give rise to the disintegration of the electrode and loss of electronic contact between the Si particles.

To overcome the large volume change and thus obtain better capacity retention and cycle life for Si anodes, various approaches have been used. Among them, the most promising approach is to create a nanocomposite structure in which nanosized Si particles are homogeneously dispersed in a ductile and active matrix.[8−12] A relatively low mass, good electronic conductivity, reasonable Li-insertion capability, and small volume expansion coupled with softness and compliance make carbon the best active matrix.[13,14]

Various methods have been employed for preparing silicon−carbon (Si−C) composite anodes. On the basis of their preparation methods, they can be mainly classified into five categories, i.e., pyrolysis[15] or chemical/thermal vapor deposition,[16] ball milling[17] or mechanical milling,[18] combination of pyrolysis and mechanical milling,[19] chemical reaction of gels,[20] and other methods such as dehydration of a carbon precursor.[21] Although all these methods provide better cycling performance for the Si−C composite anodes compared to that of pure Si anodes, capacity fading has still been unavoidable. The most probable reason for this phenomenon is the lack of a homogeneous carbon-coating layer on the surface of the Si nanoparticles and, if possible, on each individual Si nanoparticle.[22] This will increase the chances of having electrical contact to the Si nanoparticles even in case of crystal degradation of the Si nanoparticles (upon prolonged cycling). On simple admixing of carbon with Si nanoparticles, this would be less probable, but if one always has some carbon on the surface of the Si

* Corresponding author. E-mail: see-how.ng@psi.ch. Phone: +41 56 310 4406. Fax: +41 56 310 4415.

† Institute for Superconducting and Electronic Materials.

‡ ARC Center of Excellence for Electromaterials Science.

§ Faculty of Engineering.

Present address: Electrochemistry Laboratory, Paul Scherrer Institute, CH-5232 Villigen PSI, Switzerland.

10.1021/jp072778d CCC: $37.00
Published on Web 07/04/2007

nanoparticles, the electrical contact could be kept even if the Si crystal lattice breaks up.

In an earlier study, we reported preliminary electrochemical results on the carbon-coated Si nanocomposites (with 44 wt % Si content) produced via a low-temperature spray pyrolysis process in air. The nanocomposites exhibited excellent cyclability and retained a specific capacity of 1489 mA·h g^{-1} after 20 cycles.[23] Herein, we report in detail on the effects of the spray pyrolysis processing temperature on the amorphous carbon content, the thickness of the carbon-coating layer, and the homogeneity of the carbon coating. The influence of these parameters on the electrochemical performance of carbon-coated Si nanocomposites as high-capacity anode materials for Li-ion batteries will also be studied and compared accordingly.

2. Experimental Section

2.a. Materials Synthesis. Citric acid ($C_6H_8O_7$, Sigma Aldrich) was dissolved in 200 mL of absolute ethanol (99.99 wt %, Merck) under continuous stirring. Subsequently, nanocrystalline Si powder (<100 nm, Nanostructured and Amorphous Materials Inc.) was mixed into the initial citric acid/ethanol solution in the weight ratio (Si/citric acid) of 1:10, via ultrasonication for 90 min. Three types of nanocomposite materials were prepared in situ via spraying of the Si/citric acid/ethanol suspensions at 300, 400, and 500 °C, in air, using a flow rate of 4 mL min^{-1} in a vertical-type spray pyrolysis reactor. In this instance, citric acid was chosen as the carbon source, due to its low decomposition temperature (175 °C) and low oxygen content. Meanwhile, ethanol acts not only as an efficient solvent but also as a reducing agent to protect the nanocrystalline Si particles from oxidation during the spray pyrolysis process. The spray pyrolysis reaction of Si in citric acid/ethanol solution can be expressed as eq 1:

$$\mathrm{Si} + \mathrm{C_6H_8O_7/C_2H_6O} \xrightarrow{T\,^{\circ}\mathrm{C}} \mathrm{Si{-}C} + \mathrm{CO_2}\uparrow + \mathrm{H_2O}\uparrow + \mathrm{energy}\uparrow \quad (1)$$

The term "energy" in eq 1 refers to the energy released during the decomposition of the citric acid/ethanol solution into carbon and water vapor. This energy is released to the atmosphere, as the decomposition process is an exothermic reaction.

2.b. Composition and Structure Determination. The powders were characterized by X-ray diffraction (XRD) using a Philips PW1730 diffractometer with Cu Kα radiation and a graphite monochromator. Transmission electron microscopy (TEM) investigations were performed using a JEOL 2011 200 keV analytical electron microscope. TEM samples were prepared by deposition of ground particles onto lacey carbon support films. Morphologies of carbon-coated Si nanocomposite materials were investigated using a JEOL JSM 6460A scanning electron microscope (SEM). Precise carbon contents in the spray-pyrolyzed carbon-coated Si nanocomposites were determined by thermogravimetric analysis (TGA) via Setaram 92 equipment.

2.c. Electrode Preparation and Coin Cell Assembly. The anode was prepared by mixing nanocrystalline Si, carbon-coated Si nanocomposites, or spray-pyrolyzed amorphous carbon as active materials with 10 wt % carbon black (Super P, Timcal, Belgium) and 10 wt % polyvinylidene fluoride (PVDF, Sigma-Aldrich) binder in *N*-methyl-2-pyrrolidinone (NMP, Sigma-Aldrich, anhydrous, 99.5%) solvent to form a homogeneous slurry, which was then spread onto a copper foil, which serves as a current collector. The typical active mass loading of the electrodes was 2−3 mg cm^{-2}. Subsequently, the coated electrodes (average thickness of ∼50 μm) were dried in a vacuum oven at 110 °C for 24 h and then pressed to enhance the contact between the active materials and the conductive carbon. The electrochemical characterizations were carried out using coin cells. CR 2032 coin-type cells were assembled in an argon-filled (O_2 and H_2O levels less than 1 ppm) glovebox (Mbraun, Unilab, Germany) by stacking a porous polypropylene separator containing liquid electrolyte between the carbon-coated Si electrode and a lithium foil counter electrode. The electrolyte used was 1 M $LiPF_6$ in a 50:50 (w/w) mixture of ethylene carbonate (EC) and dimethyl carbonate (DMC) provided by MERCK KgaA, Germany.

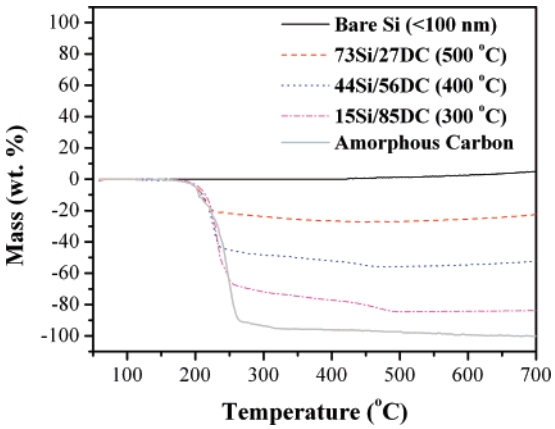

Figure 1. TGA curves of nanocrystalline Si precursor powder, carbon-coated Si nanocomposites spray-pyrolyzed in air at 500, 400, and 300 °C, and amorphous carbon spray-pyrolyzed from citric acid at 400 °C in air. The ratio Si/DC refers to the ratio of the amount of silicon over the estimated amount of disordered carbon in the spray-pyrolyzed nanocomposites from the TGA curves.

2.d. Electrochemical Measurements. The cells were galvanostatically discharged and charged in the range of 0.02−1.20 V at a constant current density of 100 mA g^{-1} via a Neware battery tester. The ac impedance spectroscopy measurements were carried out using a CHI 660A electrochemical workstation system (CH Instrument, Cordova, TN) by applying a sine wave of 5 mV amplitude over a frequency range of 100.00 kHz to 0.01 Hz. All impedance measurements were carried out in the fully delithiated state (state of charge).

3. Results and Discussion

3.a. Estimation of the Amount of Amorphous Carbon in the Carbon-Coated Si Nanocomposites. For quantifying the amount of amorphous carbon in the carbon-coated Si nanocomposite materials, TGA was carried out in air. The samples were heated from 50 to 700 °C at a rate of 5 °C min^{-1}. Figure 1 shows the TGA curves of the carbon-coated Si nanocomposite samples along with those of nanocrystalline Si powders and amorphous carbon spray-pyrolyzed in air at 400 °C. As can be seen from Figure 1, nanocrystalline Si powder starts to oxidize slowly in air at temperatures above 500 °C, with rapid oxidation above 600 °C. Meanwhile, the carbon-coated Si nanocomposite materials show rapid mass loss between 150 and 480 °C. As the nanocrystalline Si powder remains stable in this temperature range, any weight change corresponds to the oxidation of amorphous carbon. Therefore, the change in weight before and after the oxidation of carbon directly translates into the amount of amorphous carbon in the carbon-coated Si nanocomposites. With the use of this method, it was estimated that the amount of pyrolyzed carbon in the composites was 84.6, 56.0, and 27.4 wt % for the precursor solutions with weight ratios (Si/citric

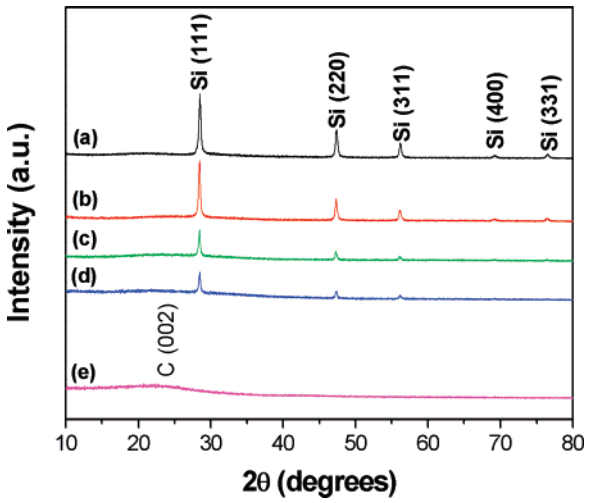

Figure 2. X-ray diffraction patterns of (a) nanocrystalline Si precursor powder, carbon-coated Si nanocomposites spray-pyrolyzed in air at (b) 500 °C, (c) 400 °C, and (d) 300 °C, and (e) amorphous carbon spray-pyrolyzed from citric acid at 400 °C in air.

TABLE 1: Theoretical and Estimated Carbon Content in Carbon-Coated Si Nanocomposites Spray-Pyrolyzed from a Nano-Si/Citric Acid/Ethanol Starting Solution at Different Processing Temperatures[a]

temp (°C)	theor wt % of carbon[b]	estimated wt % of carbon (via TGA)	mass loss % of carbon during spray pyrolysis[c]
300	78.95	84.60	−7.16
400	78.95	55.98	29.09
500	78.95	27.44	65.24

[a] Citric acid = $C_6H_8O_7$. [b] The calculation of "theor wt % of carbon" is based on the weight ratio1:10 for the nano-Si/citric acid solution and also the assumption that all carbon content in the ethanol solvent is decomposed to carbon dioxide during spray pyrolysis. [c] Mass loss (%) of carbon is calculated based on the following equation:

$$\text{mass loss}(\%) = \frac{\text{theor wt }(\%) - \text{estimated wt }(\%)}{\text{theor wt }(\%)} \times 100$$

acid) of 1:10, spray-pyrolyzed in air at 300, 400, and 500 °C, respectively. Table 1 summarizes the estimated carbon content in the spray-pyrolyzed carbon-coated Si nanocomposites. The carbon concentrations obtained after spray pyrolysis were below the targeted levels, except for the carbon-coated Si nanocomposite sample spray-pyrolyzed at 300 °C, which shows a higher value than the theoretical value. This might be due to the presence of impurities in the form of undecomposed citric acid in the sample. Therefore, temperatures above 300 °C are needed in order to fully decompose the citric acid during the spray pyrolysis process.

3.b. Structure and Morphology Analysis of Carbon-Coated Si Nanocomposites. Figure 2 shows XRD patterns of nanocrystalline Si precursor powders (Figure 2a) purchased from Nanostructured and Amorphous Materials Inc., (Figure 2b−d) carbon-coated Si nanocomposites spray-pyrolyzed in air at different processing temperatures, and (Figure 2e) spray-pyrolyzed amorphous carbon powder made from the citric acid/ethanol solution. The diffraction peak positions for all the Si-based samples (XRD patterns a−d in Figure 2) are consistent with that of pure silicon phase (JCPDS 01-0787). No obvious peaks corresponding to bulk SiO_2 or SiC crystalline phase are observed in the diffraction patterns (Figure 2b−d). This confirms that all the Si-based samples spray-pyrolyzed in air were not oxidized during the spray pyrolysis process. Moreover, no diffraction lines corresponding to crystalline carbon (graphite) were observed, indicating the amorphous nature of the carbon in the nanocomposites. Finally, XRD pattern e in Figure 2 shows a broad peak at ∼23 °, indicating the formation of amorphous carbon phase in the spray-pyrolyzed citric acid sample.

Scanning electron microscopy SEM images of the carbon-coated Si nanocomposites are shown in Figure 3. From SEM observations of the carbon-coated Si nanocomposites spray-pyrolyzed in air at 400 °C (Figure 3a), it was revealed that the particles are mainly spherical agglomerates, which is typical for the spray process, with sizes in the range of 5−10 μm. In addition, it can also be observed (Figure 3b−d) that the carbon-coated Si nanocomposites are well connected and homogeneously distributed. However, the presence of the carbon-coating layer increases the size of the individual particles. This is apparent in the case of carbon-coated Si nanocomposites spray-pyrolyzed in air at 300 °C (Figure 3d), where the individual particles are heavily coated, resulting in large agglomerates. This might be due to the fact that the sample may contain partially undecomposed citric acid.

Figure 4 shows TEM images of the nanocrystalline Si particles (Figure 4a) and carbon-coated Si nanocomposites (Figure 4b−f). The size of the individual Si particles ranged from 10 to ∼100 nm (Figure 4a). The fine spotty rings of the associated selected area electron diffraction pattern (inset of Figure 4a) correspond to nanocrystalline Si, although additional diffuse contrast within the diffraction rings may also indicate the presence of minor amounts of amorphous Si. The nanocrystalline Si particles were generally spheroidal in shape, although some of the larger ones were faceted. Figure 4b shows a typical image of the carbon-coated Si nanocomposites, where almost every individual Si nanoparticle is surrounded with a layer of carbon coating. The thickness of the carbon-coating layer increases with decreasing processing temperature, i.e., carbon coating is thickest (∼40 nm) when spray-pyrolyzed at 300 °C (Figure 4c) and thinnest (∼1 nm) when spray-pyrolyzed at 500 °C (Figure 4e). The carbon-coating layer thickness (∼10 nm) for samples spray-pyrolyzed at 400 °C (Figure 4d) can be considered optimum, as the spheroidal Si nanoparticles are homogeneously surrounded by an amorphous carbon layer. The high-resolution TEM image in Figure 4f clearly demonstrates the coexistence of two phases, i.e., the crystalline Si phase and the amorphous carbon phase.

3.c. Electrochemical Performance of Carbon-Coated Si Nanocomposites. The electrochemical performance of the nanocrystalline Si and carbon-coated Si nanocomposite electrodes was systematically investigated. Figure 5 shows the first electrochemical lithiation/delithiation of the nanocrystalline Si and carbon-coated Si nanocomposites electrodes. Different phenomena can be easily distinguished in these curves. At potentials from approximately 1.5 to 0.5 V versus Li/Li^+, the passivation film, also known as the solid/electrolyte interphase (SEI), is formed by the irreversible reduction of electrolyte on the surface of the active material, involving the formation of a lithium-ion conductive but electrolyte-blocking adhering layer.[24] As can be observed from Figure 5, the irreversible capacity contribution in this SEI formation region increased with increasing amorphous carbon content in the nanocomposite electrodes. A distinct plateau at potentials negative to 200 mV versus Li/Li^+ can be observed for the lithium alloying with the silicon active materials. Upon the following delithiation of the active materials, a plateau at around 300 mV versus Li/Li^+ can be observed, which can be attributed to the beginning of the lithium dealloying from the silicon particles. The first

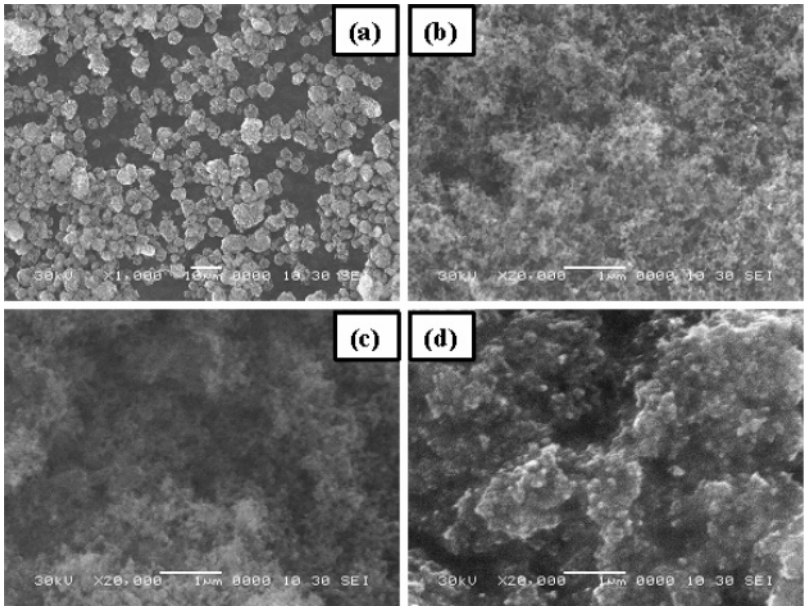

Figure 3. SEM images of carbon-coated Si nanocomposites spray-pyrolyzed in air at (a) 400 °C (low-magnification image), (b) 500 °C, (c) 400 °C, and (d) 300 °C.

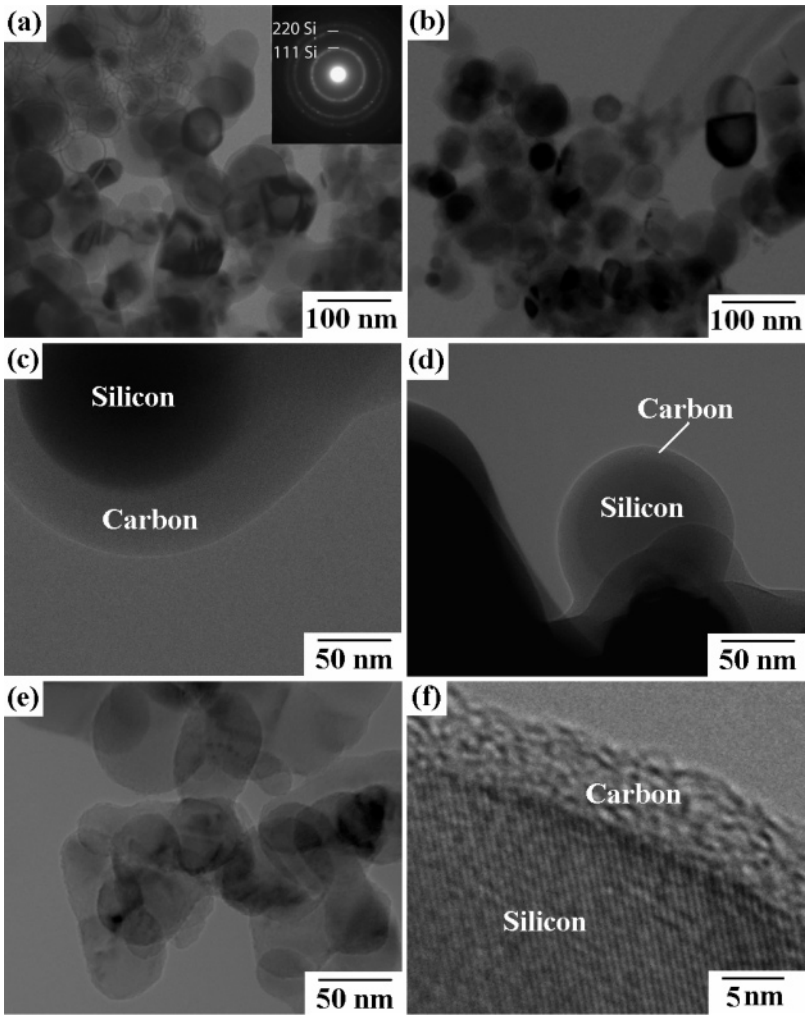

Figure 4. TEM images of nanocrystalline Si (a) and carbon-coated Si nanocomposites (b−f). Low-magnification image of (a) nanocrystalline Si, with the indexed diffraction pattern (inset) confirming the presence of Si particles and (b) carbon-coated Si nanocomposites spray-pyrolyzed at 400 °C. Panels c, d, and e are TEM images of carbon-coated Si nanocomposites spray-pyrolyzed at 300, 400, and 500 °C, respectively, revealing the thickness of the carbon-coating layer for each nanocomposite. (f) High-resolution image of carbon-coated Si spray-pyrolyzed at 400 °C, clearly showing the presence of an interface between the nanocrystalline Si particle and the amorphous carbon layer.

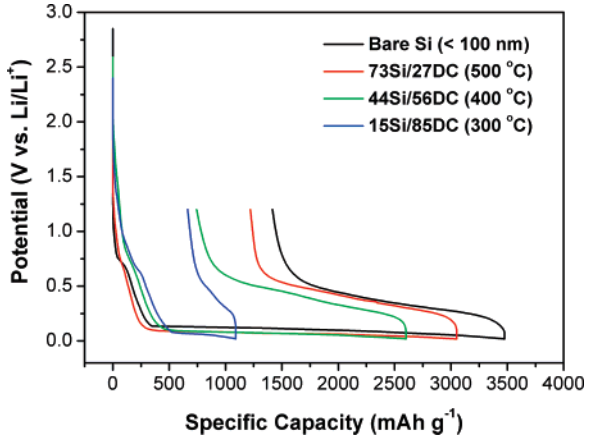

Figure 5. First discharge/charge plots of nanocrystalline Si and carbon-coated Si nanocomposite electrodes. Cycling took place between 0.02 and 1.20 V vs Li/Li^+ at a cycling rate of 100 mA g^{-1}.

cycle discharge capacities were 3474, 3050, 2600, and 1090 mA·h g^{-1} for the electrodes of nanocrystalline Si and carbon-coated Si spray-pyrolyzed in air at 500, 400, and 300 °C, respectively, with the corresponding first cycle charge capacities 2058, 1830, 1857, and 427 mA·h g^{-1}. Therefore, the first cycle Coulombic efficiencies were 59%, 60%, 71%, and 39% for the nanocrystalline Si electrode and the carbon-coated Si electrodes spray-pyrolyzed in air at 500, 400, and 300 °C, respectively.

Figure 6 summarizes the differential capacity data for the nanocrystalline Si and carbon-coated Si nanocomposite electrodes. The alloying/dealloying of lithium with Si over the potential range of 1.20−0.02 V versus Li/Li^+ yields various Li_xSi ($x < 4.4$) alloys. The first cycle differential capacity plots in Figure 6a exhibited essentially the same peak features for all electrodes below 0.3 V versus Li/Li^+. However, the first cathodic peak was shifted from 0.12 V (Si) to below 0.09 V (carbon-coated Si). This is because the SEI is different for both cases (i.e., Si/electrolyte and carbon/electrolyte, respectively). Therefore, the surface kinetics will be different, resulting in the shifted peaks that are seen in the differential capacity curves.[25] This has been confirmed by the peak shift in the SEI formation region, as shown in the inset of Figure 6a. The above-mentioned results clearly demonstrate the presence of an amorphous carbon masking layer. The 2nd, 5th, 10th, and 20th cycle differential capacity plots for the carbon-coated Si nanocomposite electrodes are shown in Figure 6b−d. It can be seen that the electrode composed of carbon-coated Si nanocomposite spray-pyrolyzed in air at 400 °C (Figure 6c) maintained high activity and reversibility, even after 20 cycles, whereas the electrodes composed of carbon-coated Si nanocomposite spray-pyrolyzed in air at 500 °C (Figure 6b) and 300 °C (Figure 6d) show severe capacity fading and loss of kinetics with cycling.

Figure 7 shows the cycling behavior of the nanocrystalline Si and carbon-coated Si nanocomposite electrodes. The calculated capacities were solely based on the active electromaterial,

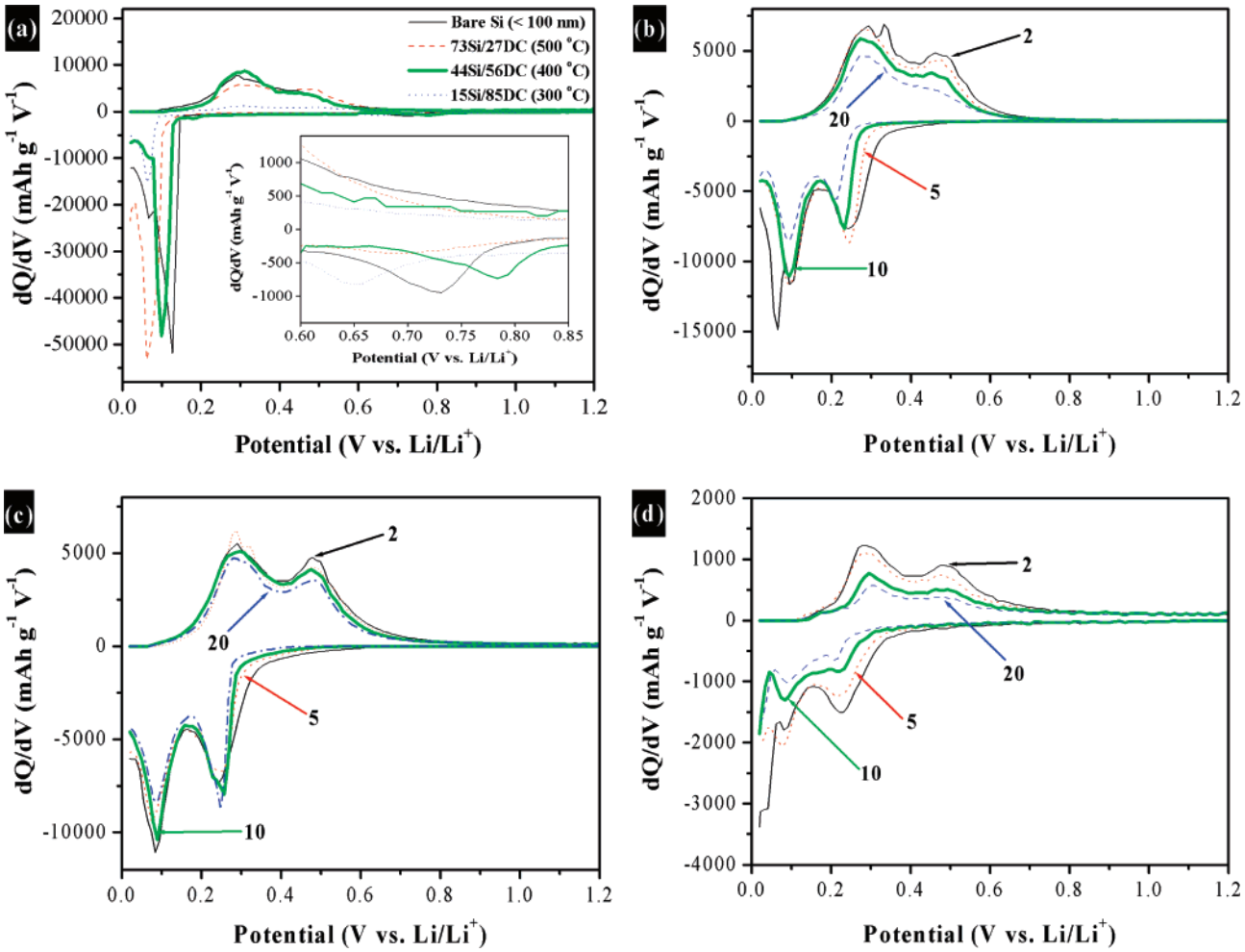

Figure 6. (a) First cycle differential capacity plots of nanocrystalline Si and carbon-coated Si nanocomposites electrodes (inset: enlarged plot of (a)). Panels b, c, and d are differential capacity plots for carbon-coated Si nanocomposites spray-pyrolyzed at 500, 400, and 300 °C, respectively, with the numbers indicating the cycle number. Cycling took place between 0.02 and 1.20 V vs Li/Li^+ at a cycling rate of 100 mA g^{-1}.

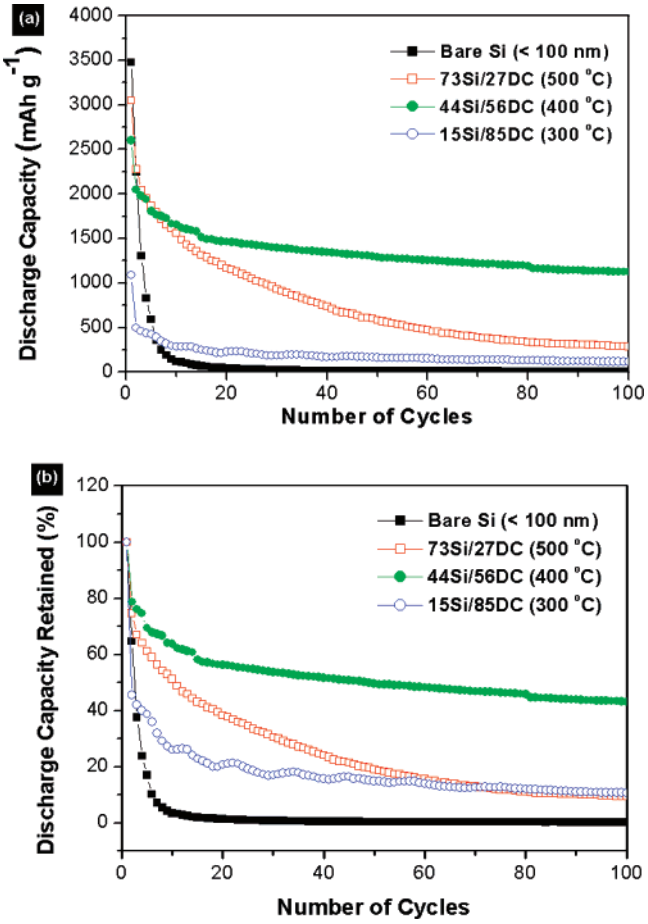

Figure 7. (a) Cycle life of nanocrystalline Si and carbon-coated Si nanocomposites electrodes cycled between 0.02 and 1.20 V vs Li/Li$^+$ at a cycling rate of 100 mA g^{-1}. (b) The corresponding capacity retained compared to the first discharge capacity in (a).

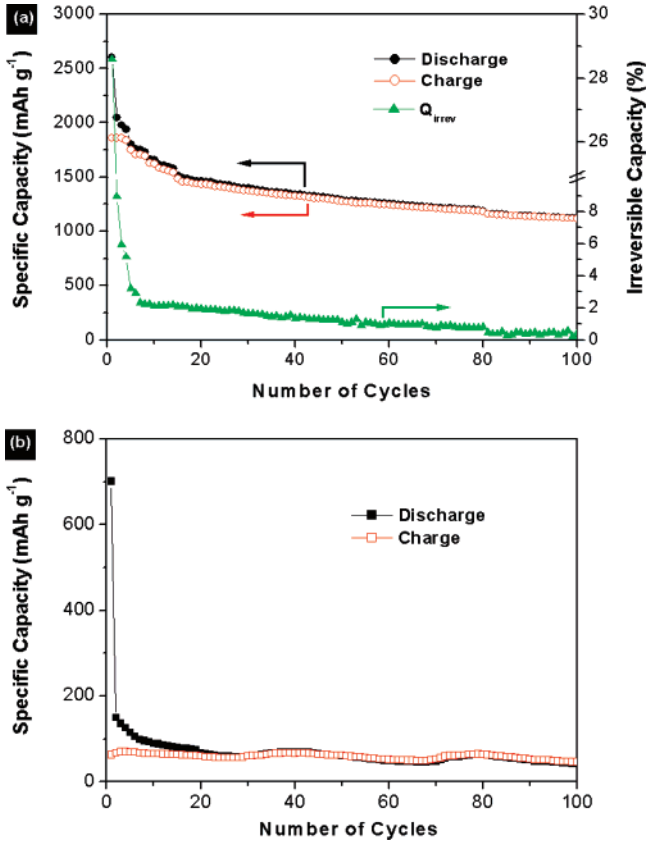

Figure 8. Cycling behavior for electrodes of (a) carbon-coated Si nanocomposites spray-pyrolyzed at 400 °C, with 44 wt % Si content and (b) amorphous carbon spray-pyrolyzed at 400 °C. Cycling took place between 0.02 and 1.20 V vs Li/Li$^+$ at a cycling rate of 100 mA g^{-1}.

i.e., Si or carbon-coated Si nanocomposite particles in the electrodes. With the use of a nonrestricted cycling procedure, the initial reversible capacities (second discharge capacity) were 2247, 2276, 2045, and 497 mA·h g^{-1} for the electrodes composed of nanocrystalline Si and of carbon-coated Si spray-pyrolyzed in air at 500, 400, and 300 °C, respectively. Subsequently, the discharge capacities beyond 100 cycles were maintained at 10, 288, 1120, and 116 mA·h g^{-1} for the nanocrystalline Si electrode and the carbon-coated Si electrodes spray-pyrolyzed in air at 500, 400, and 300 °C, respectively, corresponding to the ratios of the specific capacities retained after 100 cycles to the first discharge capacities, which are 0.3%, 9%, 43%, and 11%, respectively. These results show that the optimum carbon-coating content is slightly above 50% by weight, as demonstrated by the nanocomposite spray-pyrolyzed in air at 400 °C.

Figure 8 shows the cycling behavior of the carbon-coated Si nanocomposite electrode with 44 wt % Si content and the corresponding cycling behavior of the amorphous carbon prepared by spray pyrolysis of the citric acid/ethanol solution at 400 °C in air. The carbon-coated Si nanocomposite electrode shows a moderate capacity fading behavior in the first 20 cycles, followed by a relatively flat and low capacity fading behavior for the next 80 cycles. The carbon-coated Si nanocomposite electrode shows an irreversible capacity loss (Q_{irrev}) of less than 0.4% per cycle. However, the capacity fading behavior shown in the first 20 cycles can be attributed to the high irreversible capacity contributed by the presence of a large amount of amorphous carbon content in the nanocomposite electrode. This is clearly demonstrated in Figure 8b, where the electrochemical lithiation/delithiation into/from amorphous carbon is illustrated. In the first cycle, the insertion capacity of the amorphous spray-pyrolyzed carbon is approximately 700 mA·h g^{-1}. Since the carbon content in the carbon-coated Si electrode is 56 wt %, the insertion capacity can account to a large extent for the low Coulombic efficiency of the carbon-coated Si electrode in the first cycle (see Figure 8a). The low discharge capacity (~40 mA·h g^{-1}) of the amorphous carbon after 100 cycles suggests that the degree of carbonization is very low. This may be due to the instantaneous nature of the spray pyrolysis process, which normally takes only a few minutes to produce the spray-pyrolyzed powder.[14] Meanwhile, by subtracting the capacity contributed by the amorphous carbon (~40 mA·h g^{-1} after 100 cycles), the discharge capacity delivered by the Si active mass (44 wt %) was estimated to be approximately 1098 mA·h. Therefore, the specific capacity of Si in the nanocomposite electrode was calculated to be 2495 mA·h g^{-1} after 100 cycles, which amounts to an impressive 60% of the theoretical value (4200 mA·h g^{-1}). This shows the beneficial effect of the carbon coating on the enhanced dimensional stability of the Si particles during the Li alloying/dealloying process, which not only buffered the great volume changes during the cycling process, but also avoided possible agglomeration of the uniformly distributed silicon particles.[26−28]

In order to verify the effect of carbon coating on the electronic conductivity of the nanocomposites, ac impedance measurements were conducted. The Nyquist plots obtained are compared in Figure 9 for the nanocrystalline Si (Figure 9a) and carbon-coated Si nanocomposite spray-pyrolyzed at 400 °C (Figure 9b) electrodes after 1 and 100 cycles. The thickness of the electrodes

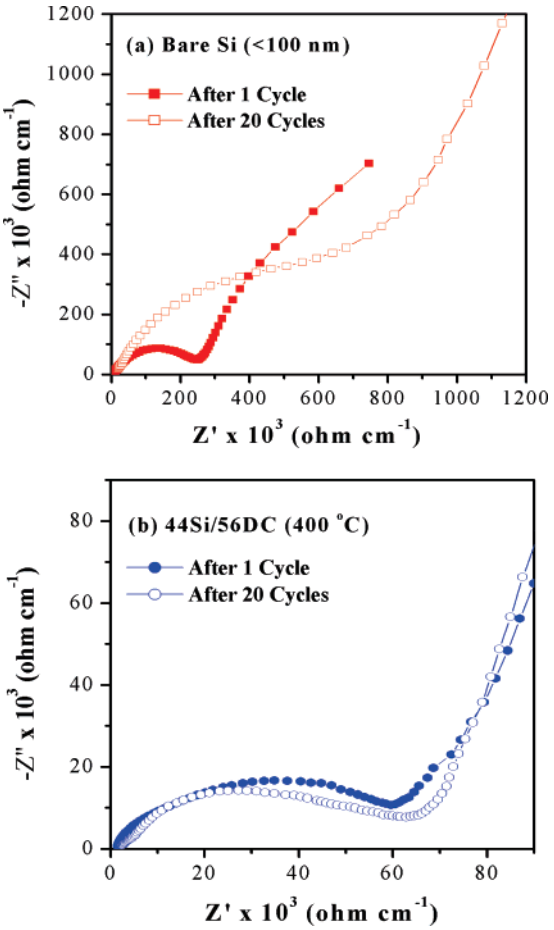

Figure 9. Impedance plots for electrodes of (a) nanocrystalline Si and (b) carbon-coated Si nanocomposite spray-pyrolyzed at 400 °C. All measurements were conducted in the delithiated state.

was maintained at 50 μm and the coated area of the electrodes at 1 cm^2. To maintain uniformity, electrochemical impedance spectroscopy (EIS) experiments were performed on working electrodes in the fully charged (delithiated) state. In general, one semicircle in the high-frequency range was observed for all the samples. The diameter of the semicircle represents the interparticle contact resistance.[29] Meanwhile, in the low-frequency region, an angled straight line was obtained, which represents a diffusion-controlled process in the SEI.[30] In addition, we found that the diameter of the semicircles was enlarged after 100 cycles for all the samples. However, when Figure 9a is compared to Figure 9b, considerable differences are observed. The diameter of the semicircle after 100 cycles increased by more than 200% (from 250 to 750 kΩ cm^{-1}) in the case of nanocrystalline Si electrodes compared to only an increase of approximately 17% (from 60 to 70 kΩ cm^{-1}) for the electrodes of carbon-coated Si nanocomposite spray-pyrolyzed at 400 °C. Therefore, it can be assumed that the interparticle contact resistance was suppressed with the carbon coating, resulting in better cycling of the cells during the charge/discharge process.[29]

4. Conclusions

A series of carbon-coated Si nanocomposites have been successfully synthesized via in situ spray pyrolysis of Si/citric acid/ethanol solution in air with a flow rate of 4 mL min^{-1} at three different processing temperatures, i.e., at 300, 400, and 500 °C. The spray-pyrolyzed powders are fine nanocrystalline Si homogeneously coated with an amorphous carbon layer. The thickness of the carbon-coating layer increased with decreasing processing temperature. The amorphous carbon content estimated by TGA shows that a small amount of impurities was present in the form of undecomposed citric acid for the carbon-coated Si nanocomposite spray-pyrolyzed in air at 300 °C. Both the XRD and TEM results indicate that there was no bulk SiO_2 or SiC crystalline phase detected in the spray-pyrolyzed nanocomposites. The alloying and dealloying of lithium with Si over the 1.20−0.02 V range yields various Li_xSi ($x < 4.4$) alloys. The discharge capacity of carbon-coated Si nanocomposite spray-pyrolyzed in air at 400 °C is 1120 mA·h g^{-1} after 100 cycles, corresponding to the Si active mass contributing a specific capacity of 2495 mA·h g^{-1}. The carbon-coated Si nanocomposite electrodes show an improved cycle life compared to that of the pure Si electrode. We strongly believe that the presence of the carbon-coating layer is responsible for the enhanced dimensional stability of the Si particles during the Li alloying/dealloying processes, which then significantly improved the electrical conductivity of the composites. In summary, spheroidal carbon-coated Si nanocomposite, prepared via a spray pyrolysis method in air, is a promising candidate for use as an anode material in the lithium-ion battery, as it has excellent specific capacity retention, high Coulombic efficiency, and low cost due to the abundance of both Si and carbon sources.

Acknowledgment. This research was supported in part by ARC Center of Excellence funding under Grant No. CE0561616 administered through the University of Wollongong. Many thanks also go to Dr. K. Konstantinov for his assistances in the spray pyrolysis process and Dr. Z. P. Guo for fruitful scientific discussions. Finally, the authors are grateful to Dr. T. Silver for critical reading of the manuscript.

References and Notes

(1) Tarascon, J. M.; Armand, M. *Nature* **2001**, *404*, 359.
(2) Weydanz, W. J.; Wohlfahrt-Mehrens, M.; Huggins, R. A. *J. Power Sources* **1999**, *82*, 237.
(3) Idota, Y.; Kubota, T.; Matsufuji, A.; Maekawa, Y.; Miyasaka, T. *Science* **1997**, *276*, 1395.
(4) Winter, M.; Besenhard, J. O.; Spahr, M. E.; Novak, P. *Adv. Mater.* **1998**, *10*, 725.
(5) Lee, S. J.; Lee, J. K.; Chung, S. H.; Lee, H. Y.; Lee, S. M.; Baik, H. K. *J. Power Sources* **2001**, (97−98), 191.
(6) Sharma, R. A.; Seefurth, R. N. *J. Electrochem. Soc.* **1976**, *123*, 1763.
(7) Boukamp, B. A.; Lesh, G. C.; Huggins, R. A. *J. Electrochem. Soc.* **1981**, *128*, 725.
(8) Kim, H.; Choi, J.; Sohn, H.; Kang, T. *J. Electrochem. Soc.* **1999**, *146*, 4401.
(9) Roberts, G. A.; Cairns, E. J.; Reimer, J. A. *J. Power Sources* **2002**, *110*, 424.
(10) Wu, X.; Wang, Z.; Chen, L.; Huang, X. *Electrochem. Commun.* **2003**, *5*, 935.
(11) Beaulieu, L. Y.; Hewitt, K. C.; Turner, R. L.; Bonakdarpour, A.; Abdo, A. A.; Christensen, L.; Eberman, K. W.; Krause, L. J.; Dahn, J. R. *J. Electrochem. Soc.* **2003**, *150*, A149.
(12) Asao, M.; Kawakami, S.; Ogura, T. U.S. Patent Application 2004/0248011, 2004.
(13) Kurita, N.; Endo, M. *Carbon* **2002**, *40*, 253.
(14) Ng, S. H.; Wang, J.; Konstantinov, K.; Wexler, D.; Chen, J.; Liu, H. K. *J. Electrochem. Soc.* **2006**, *153*, A787.
(15) Wilson, A. M.; Reimers, J. N.; Fuller, E. W.; Dahn, J. R. *Solid State Ionics* **1994**, *74*, 249.
(16) Holzapfel, M.; Buqa, H.; Scheifele, W.; Novak, P.; Petrat, F. M. *Chem. Commun.* **2005**, *12*, 1566.
(17) Wang, C. S.; Wu, G. T.; Zhang, X. B.; Qi, Z. F.; Li, W. Z. *J. Electrochem. Soc.* **1998**, *145*, 2751.
(18) Liu, Y.; Hanai, K.; Horikawa, K.; Imanishi, N.; Hirano, A.; Takeda, Y. *Mater. Chem. Phys.* **2004**, *89*, 80.

(19) Guo, Z. P.; Milin, E.; Wang, J. Z.; Chen, J.; Liu, H. K. *J. Electrochem. Soc.* **2005**, *152*, A2211.

(20) Hasegawa, T.; Mukai, S. R.; Shirato, Y.; Tamon, H. *Carbon* **2004**, *42*, 2573.

(21) Yang, X.; Wen, Z.; Zhu, X.; Huang, S. *Electrochem. Solid-State Lett.* **2005**, *8*, A481.

(22) Kasavajjula, U.; Wang, C.; Appleby, A. J. *J. Power Sources* **2007**, *163*, 1003.

(23) Ng, S. H.; Wang, J.; Wexler, D.; Konstantinov, K.; Guo, Z. P.; Liu, H. K. *Angew. Chem., Int. Ed.* **2006**, *45*, 6896.

(24) Holzapfel, M.; Buqa, H.; Krumeich, F.; Novak, P.; Petrat, F. M.; Veit, C. *Electrochem. Solid-State Lett.* **2005**, *8*, A516.

(25) Liu, W. R.; Wang, J. H.; Wu, H. C.; Shieh, D. T.; Yang, M. H.; Wu, N. L. *J. Electrochem. Soc.* **2005**, *152*, A1719.

(26) Larcher, D.; Mudalige, C.; George, A. E.; Poter, V.; Gharghouri, M.; Dahn, J. R. *Solid State Ionics* **1999**, *122*, 71.

(27) Dimov, N.; Kugino, S.; Yoshio, M. *Electrochim. Acta* **2003**, *48*, 1579.

(28) Liu, Y.; Matsumura, T.; Imanishi, N.; Hirano, A.; Ichikawa, T.; Takeda, Y. *Electrochem. Solid-State Lett.* **2005**, *8*, A599.

(29) Fan, J.; Fedkiw, P. S. *J. Power Sources* **1998**, *72*, 165.

(30) Li, H.; Huang, X.; Chen, L. *J. Power Sources* **1999**, (81−82), 340.